Journal of Catalysis **205,** 346–353 (2002)
doi:10.1006/jcat.2001.3462, available online at http://www.idealibrary.com on IDEAL®

In Situ XRD Study of the Influence of Thermal Treatment on the Characteristics and the Catalytic Properties of Cobalt-Based Fischer–Tropsch Catalysts

Dan I. Enache,[1,2] Bernadette Rebours, Magalie Roy-Auberger, and Renaud Revel

Institut Français du Pétrole, 1 & 4 Avenue Bois Préau, 92500 Rueil Malmaison, France

Received July 9, 2001; revised November 6, 2001; accepted November 6, 2001

***In situ* X-ray diffraction analysis was performed for several thermal treatment protocols for zirconia- and alumina-supported cobalt catalysts. Zirconia support was found to promote amorphous or poorly crystalline hexagonal metallic cobalt. At the same time, the direct reduction of nitrate precursor leads to weaker metal-support interactions than in the case of calcined catalysts and increases the quantity of amorphous or poorly crystalline hexagonal metallic cobalt, which are assumed to be the active phases in the Fischer–Tropsch synthesis. The airflow calcination yields crystallised Co_3O_4, which is more difficult to reduce. Moreover, reduction of crystallised Co_3O_4 promotes formation of cubic cobalt, which is less active than hexagonal cobalt in Fischer–Tropsch synthesis.**

Key Words: **cobalt; zirconia; alumina; *in situ* XRD; reducibility; Fischer–Tropsch synthesis.**

1. INTRODUCTION

Cobalt-based catalysts are widely used in Fischer–Tropsch synthesis (FTS). The goal of this reaction is to form linear aliphatic hydrocarbons with a broad molecular weight distribution, typical of polymerisation processes (1, 2). The catalyst preparation method and the pretreatment conditions used for these catalysts are known to have great influence on the surface states of cobalt and cobalt oxide species formed, thus determining the catalytic properties. A number of studies have been reported concerning the effect of pretreatment conditions on catalysts containing cobalt (3–7).

A few studies have focused on the effect of reduction temperature on the performance of Co/Al_2O_3 catalysts (8–10) or Ru-promoted Co/Al_2O_3 (4). Continuing research in the same area, Iglesia (11) showed that the elimination of the calcination step, by reducing nitrate precursors directly in flowing hydrogen, led to an increase in Co dispersion. Moreover, the use of high hydrogen-flow rates and slow temperature ramping protocols led to additional improvements in cobalt dispersion, even for high Co concentration (11).

Another factor that may influence activity and selectivity in Fischer–Tropsch synthesis is the nature of the support used. The role of the support is to disperse the active phase. It must present good mechanical properties (resistance to attrition) and good thermal stability. The types of support generally used are oxides such as Al_2O_3, SiO_2, and TiO_2 and less frequently carriers such as MgO, coal, or polymers. In this context, Reuel and Bartholomew showed the catalytic activity of cobalt catalysts to be a function of the nature of the support (12), decreasing in the order

$$Co/TiO_2 > Co/Al_2O_3 > Co/SiO_2 > 100\%\ Co > Co/MgO.$$

Some authors claim that the surface of big metallic cobalt particles is enriched in electrons. It also seems that the adsorption of CO molecules is influenced by metallic cluster size (13). Also, by increasing metal dispersion, production of light hydrocarbons is favoured (14), and consequently, decreasing the dispersion leads to an increase in the molecular weight of reaction products (10, 12).

Iglesia *et al.* (15) claimed that for high conversions and pressures over 5 bar, the influence of the support on the activity for methane and hydrocarbons of greater chain length than C_{5+} could be neglected. He found that C_{5+} selectivity is insensitive for cobalt dispersions between 0.5 and 9.5%. Moreover, the reaction is insensitive to the dispersion and the structure of cobalt. This is confirmed in further studies by Geerlings *et al.* (16) on Co monocrystals. Another study (17) reveals that the hydrocarbon distribution resulting from the reaction is a function of metal reduction degree, which is itself a function of the interaction between cobalt and carrier and of cobalt crystal size.

Recent studies reveal a growing interest in catalysts supported on zirconia-coated alumina or silica (18–20), in pure zirconia (21, 22), and in the influence of ZrO_2 as a promoter in Fischer–Tropsch synthesis (18–20, 22).

[1] To whom correspondence should be addressed. Fax: 44/029-2087-4075. E-mail: enachedi@cf.ac.uk.

[2] Current address: 16 Richmond Road, Roath, CF24 3AS, Cardiff, United Kingdom.

0021-9517/02 $35.00

In this study we describe the effect of the thermal treatment of zirconia- and alumina-supported catalysts with respect to activity, selectivity, and X-ray diffraction (XRD) patterns.

2. EXPERIMENTAL

2.1. Catalyst Preparation

The supported cobalt catalysts used in this study were prepared by incipient wetness impregnation of Co(II) nitrate. Both supports were first treated by calcination under airflow at 500°C and had the following characteristics: A1 was gamma Al_2O_3, SCCa-5/170 from Condea, with a specific surface area of 173 m^2/g and a pore volume of 0.49 cm^3/g; and Z1 was monoclinic ZrO_2 from Mel Chemicals, with a specific surface area of 100 m^2/g, and a pore volume of 0.26 cm^3/g.

The impregnated supports were dried at 120°C for 2 h.

The catalysts are referenced using the percentage and name of the active phase (e.g., 10Co), followed by the name of the support and a symbol relative to the treatment. These symbols are as follows:

O, Air calcination—400°C (4 h, 10°C/min); Protocol 1.

N, Nitrogen calcination—400°C (4 h, 10°C/min); Protocol 2.

H, Direct hydrogen reduction of the nitrate precursor—350°C (4 h, 5°C/min); Protocol 3.

H1, Direct hydrogen reduction of the nitrate precursor—350°C (4 h, 5°C/min), cooled to room temperature under hydrogen flow, then placed in contact with air; Protocol 4.

H2, Direct hydrogen reduction of the nitrate precursor—350°C (4 h, 1°C/min); Protocol 5. For instance, a catalyst named 10CoZ1–N contains 10% Co supported on zirconia Z1 support and was calcined under nitrogen flow.

2.2. Temperature-Programmed Reduction (TPR)

The TPR experiments were performed with a 500-mg sample of catalyst under a mixture of 10% H_2 in N_2 flowing at 30 cm^3/min, and the temperature was raised at a rate of 5°C/min until it reached 970°C. A thermal conductivity detector (TCD) was used to determine the hydrogen consumption.

2.3. Oxygen Chemisorption Experiments

The oxygen chemisorption experiments were performed in a pulse-flow apparatus after a 2-h reduction step at 350°C in hydrogen flow, followed by a hydrogen ventilation step (1 h at 350°C in argon flow), cooling to room temperature in argon flow, and then oxygen pulse chemisorption.

2.4. Transmission Electronic Microscopy (TEM)

The TEM images were obtained using a JEOL 2010 apparatus. The catalyst samples were ground and ultrasonically dispersed in ethanol. Drops of the suspension were taken from different levels and air dried on a porous carbon film.

2.5. In Situ X-Ray Diffraction Study

A D501 Siemens powder diffractometer instrument with monochromatic Cu$K\alpha$ radiation was used for the XRD measurements. The diagrams were scanned at 0.05°/step size using a 5- to 20-s acquisition time per step. The *"in situ"* sample holder was the XRK reactor cell commercialised by ANTON PAAR. In this cell, the gas flow is forced through the sample (≈0.2 g) packed on a sintered glass sieve and placed in the centre of an oven. The gas flow (hydrogen, nitrogen, etc) was fixed at 2 L/h and the heating rate at 5°C/min.

2.6. Catalytic Test

The catalytic test was carried out in a fixed-bed microreactor (0.4 g of catalyst diluted in 15 cm^3 of carborundum, in order to avoid the apparition of heat spots; $H_2/CO = 9$; $T = 230$°C; 1.5 bar total pressure, total feed-rate, 6.23 L/h). Product analysis was performed online with a Varian 3800 GC, equipped with TCD and flame ionization detector (FID) detection.

3. RESULTS AND DISCUSSION

3.1. TPR Study of 10CoZ1 Catalysts

Figure 1 shows the TPR diagrams of the 10CoZ1 catalysts after calcination under air (O) or nitrogen (N) flow at 400°C (for 4 h), or direct reduction of the Co(II) nitrate under hydrogen flow at 350°C (4 h), then cooling at room temperature and contact with atmospheric air (H1).

10CoZ1–O presents four reduction peaks and the greatest hydrogen consumption. We assume that all the cobalt deposited in this case is under Co_3O_4 form, because by XRD we find only its pattern and because the Co_2O_3 species

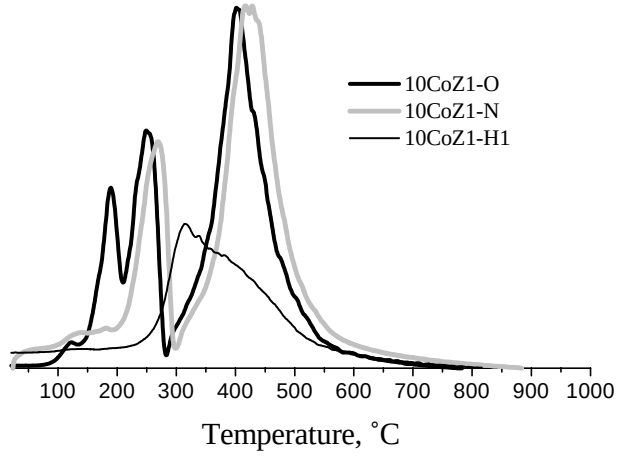

FIG. 1. TPR diagram of 10CoZ1 catalyst after different treatments.

is an unstable one. Moreover, we assume that all nitrogen compounds (nitrates, nitrites) are decomposed on this catalyst after air calcination at 400°C (5). This leads to a total cobalt balance sheet of 100%. The ratio of the surfaces for these peaks is about 1 : 12 : 20 : 67 It is generally assumed that the reduction of Co_3O_4 proceeds in two steps (29–33):

$$Co_3O_4 + H_2 \rightarrow 3CoO + H_2O,$$
$$3CoO + 3H_2 \rightarrow 3Co + 3H_2O.$$

It means that the first two peaks and about two-thirds of the third peak are generated by Co_3O_4 reduction to CoO. The last third of the third peak and the fourth peak are attributed to CoO reduction into metallic Co. In fact, in our case, we assumed that Co_3O_4 reduces in three stages, which indicates that we have three kinds of Co_3O_4 species. A recent study (23) reveals that the reduction temperature of Co_3O_4 is strongly influenced by the size of the particles. Particles with a size inferior to 53 Å are totally reduced in metallic cobalt for temperatures below 300°C. The cobalt, after reduction at 300°C, coexists in three forms (metallic, CoO, and Co_3O_4) if the initial Co_3O_4 particle size was 121 Å. The reduction peak at 420°C is ascribed to the reduction of CoO in metallic cobalt. In conclusion, TPR diagrams suggest that our samples contain Co_3O_4 particles with a wide range of sizes. The difference between TPR of the catalysts supported on zirconia (four reduction peaks) and alumina (two reduction peaks) is also linked to the inertness of zirconia. Indeed, this zirconia support does not produce cobalt zirconates (cobalt is reduced to metallic cobalt rather than to strongly interacts with the ZrO_2 carrier), while alumina produces cobalt aluminates at calcination temperatures below those necessary to reduce entirely the cobalt.

The hydrogen consumption for the 10CoZ1–N (Protocol 2) catalyst is 10% lower than for that of the 10CoZ1–O catalyst, and we assume that the cobalt oxide is a mixture of Co_3O_4 (mainly) and some CoO. In this case the first two peaks are absent, and the last two peaks are slightly shifted (10°C) to higher temperatures. The lack of the two first peaks is caused by the thermal treatment. Indeed, the most reducible species of Co_3O_4 (the first two peaks in the 10CoZ1–O case) are reduced by the gas flow, because N_2 is a slight reducing agent. Further calcination at higher temperature in nitrogen atmosphere will increase the quantity of CoO.

The 10CoZ1–H1 catalyst hydrogen consumption is 37% compared to the catalyst calcined under airflow. A single peak forms the TPR diagram, with a maximum at 300°C, indicating a stronger metal-support interaction (SMSI). This phenomena is generated by the local increase in the temperature caused by the violent and rapid oxidation of the metallic cobalt particles when the reduced catalyst is put in contact with the atmospheric air. This last thermal treatment leads to a different reduction process in the TPR analysis. XRD diagrams suggest that after this treatment, Co is in Co_3O_4 form. Nevertheless, some amount of metallic cobalt must still be present in the bulk of the particles. The size of bulk metallic cobalt particles must be small enough to be invisible in the final XRD diagram. This metallic part will allow reducing of all amounts of Co_3O_4 obtained by reoxidation under 420°C. It is the principle of metallic germination, which would begin at the centre of the particles and would diffuse to the borders (23).

TABLE 1

Cobalt Supported on Z1 Zirconia Reducible at 400°C

Catalyst	% Co reduced at $T < 400$°C	Total % Co reduced (r.t. → 1000°C)	% Co reduced at $T > 400$°C
10CoZ1–O	61	100	39
10CoZ1–N	41	90	49
10CoZ1–H	25	37	12

The influence of thermal treatment on the reducibility of the cobalt in this catalyst can be synthesised as follows. The highest quantity of cobalt species which are reducible under 400°C is observed after an airflow calcination. Calcination under nitrogen leads to a lower Co_3O_4 quantity but to a slightly higher reduction temperature. On air exposure, the catalyst directly reduced at 350°C and cooled under hydrogen shows an increase in temperature due to sudden surface reoxidation. The quantity of oxide formed is quite low, but its further reduction during TPR experiment is more difficult, due to SMSI (strong metal-support interaction). Table 1 presents the evolution of cobalt supported on Z1 zirconia reducible at 400°C.

3.2. Oxygen Chemisoption Results

The results of oxygen chemisorption with respect to thermal treatment are shown in Table 2. We used a spherical model to evaluate the size of the particles and we considered that the oxygen chemisorption yields surface Co_3O_4. We considered a value of 6.62×10^{-20} m^2 for each cobalt atom (24).

TABLE 2

Chemisorption Results for the Catalysts Supported on Zirconia and Alumina, Function of Thermal Treatment Supported by Catalysts before the Oxygen Chemisorption Analysis

Catalysts	Thermal treatment	Dispersion	$S_{Co\ exposed}$ (m^2/g)	Particle diameter (Å)
10Co/Z1–O	Protocol 1	7.5%	55	124
10Co/Z1–N	Protocol 2	7.7%	56	120
10Co/Z1–H	Protocol 3	7.8%	56	120
10Co/Z1–H1	Protocol 4	6.5%	47	143
10Co/A1–N	Protocol 2	0.7%	5.3	1280

The results show no influence of thermal treatment on the particle diameter size of cobalt supported on the same oxide, except for the reduced catalyst reoxided by contact with atmospheric air (10Co/Z1–H1). This treatment leads to an increase in particle size, from about 120 to 145 Å. All other thermal treatment (air calcination, nitrogen calcination, or direct hydrogen reduction without air contact) leads to a similar dispersion and cobalt accessible surface.

3.3. TEM Characterisation of 10CoZ1 Catalysts

The TEM images (Fig. 2) obtained after different thermal treatment agreed with the oxygen chemisorption results for the catalysts supported on the Z1 the zirconia carrier. The Co_3O_4 particle sizes, as measured by this technique, are comprised in the range 50–500 Å, which confirms the suggestion given by the TPR analysis that we have a wide distribution of Co_3O_4 particle sizes. The most frequent Co_3O_4 crystal size is 100 Å for the catalysts obtained by airflow and nitrogen-flow calcination (Protocols 1 and 2) and 150–200 Å for the sample 10CoZ1–H1 (Protocol 4). In this last case, no metallic cobalt or CoO is observed, even when the hydrogen consumption is only 37% compared to the one observed in the 10CoZ1–O case (Protocol 1—airflow calcination). This result suggests that Co_3O_4 covers all the surface of the active-phase particles (metallic cobalt obtained during the reduction step and nonreoxided, becoming invisible). Nevertheless, TPR experiment showed us that there is some metallic cobalt in the CoZ1–H1 sample.

3.4. In Situ XRD Characterisation

10CoZ1 catalyst. Figure 3 shows the XRD pattern of the 10CoZ1 catalysts reduced at 450°C, after subtraction of the support contribution for different sample thermal treatments. This temperature was chosen because no metallic Co pattern is observed at reduction temperatures below 450°C for air-calcined or nitrogen-calcined samples. Each diagram is the average of 10 sets of data, each collected during 20 s per step. This protocol ensures a good signal/noise ratio.

10CoZ1–H (direct reduction of the nitrate precursor) exhibits more hexagonal Co and less cubic Co than the 10CoZ1–O (airflow calcination) sample. The nitrogen-flow calcination leads to an intermediate situation similar to that

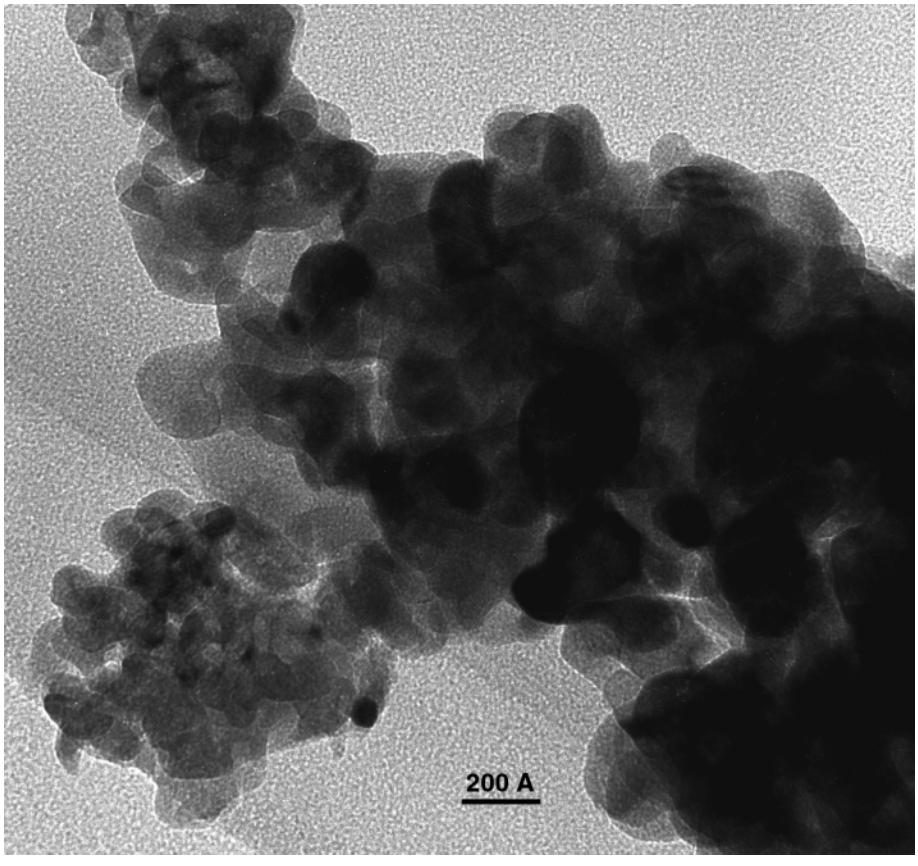

(a)

FIG. 2. TEM images of the catalysts: (a) calcined in airflow (Protocol 1—10CoZ1–O); (b) calcined in nitrogen flow (Protocol 2—10CoZ1–N); (c) direct reduction under hydrogen flow, return to room temperature, then air contact (Protocol 4—10CoZ1–H1).

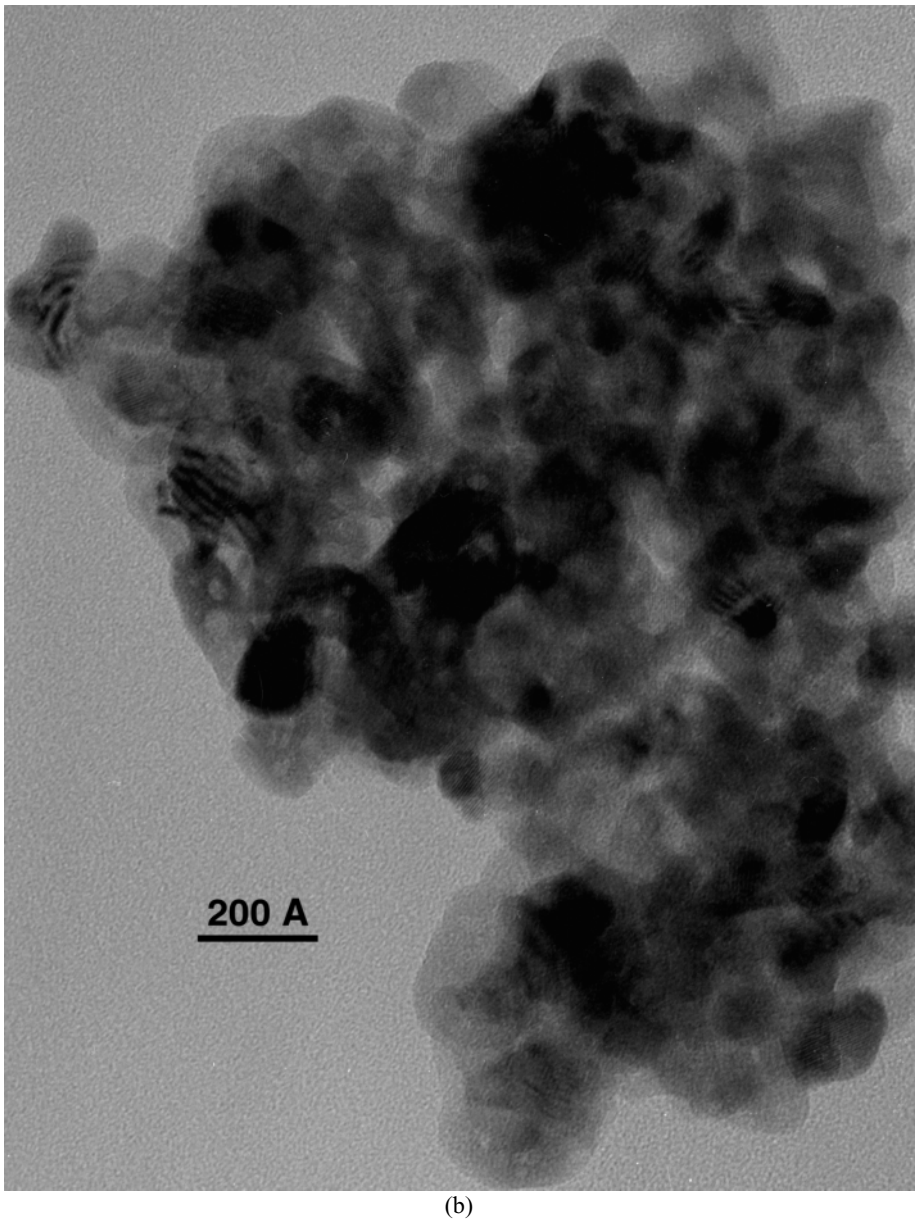

(b)

FIG. 2—*Continued*

caused by airflow calcination. The cobalt diffraction line at 44.5° is less broadened in the 10CoZ1–H sample than in the calcined samples. That means either that metallic particles are bigger or that the metallic cobalt contains fewer structural defects. Anyway, in all cases a mixture of hexagonal and cubic cobalt with structural imperfections forms the metallic phase. The metallic cobalt diffraction line shape is typical of a mixing of faulted hexagonal and cubic structures (25–27). The hexagonal/cubic stacking fraction is variable according to the treatment conditions of the sample.

Figure 4 presents the XRD diagrams of the 10CoZ1–H (direct reduction of the nitrate precursor) at different reduction temperatures. Each diagram is the mean of three sets of data, each collected with a 0.05° step size and a counting time of 5 s per step. After the subtraction of the support contribution, the diagram was smoothed using a five-average averaging protocol, in order to improve the signal/noise ratio. This operation did not displace the diffraction lines.

At 260°C we observe the presence of Co_3O_4 (diffraction line at 37°), with CoO traces. The presence of Co_3O_4 is linked with the cobalt nitrate decomposition. Before being totally reduced by the hydrogen flow, the NO_2 evolved by the precursor decomposition is susceptible to oxidised Co(II) oxide. When the reduction temperature is increased to 300°C, the Co_3O_4 disappears and transforms

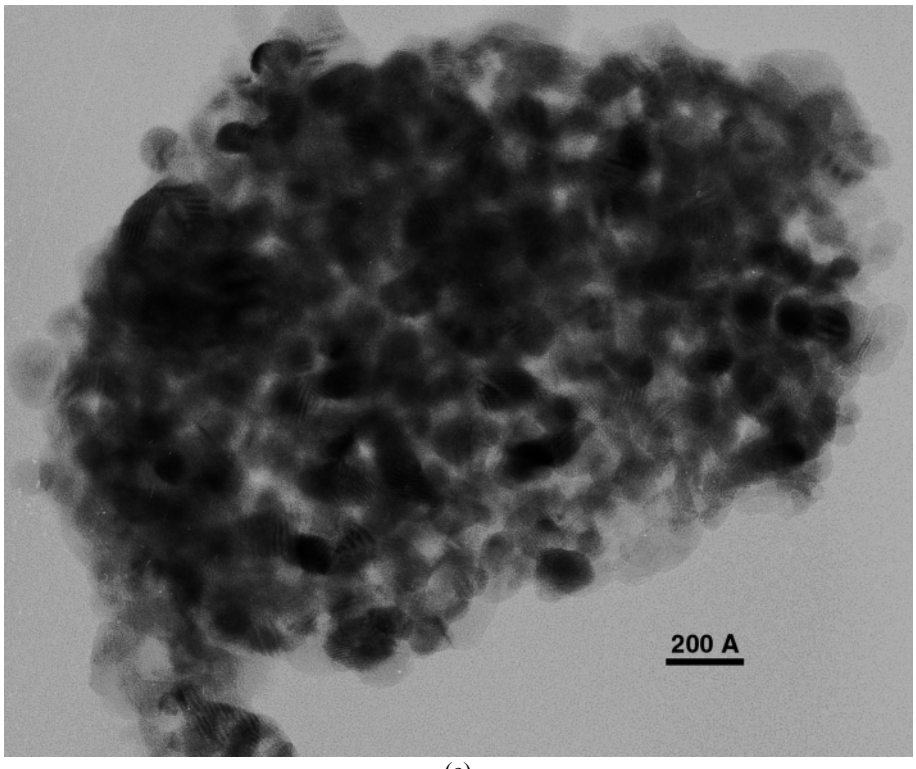

(c)

FIG. 2—*Continued*

to CoO, as evidenced by the shift of the oxide diffraction line from 37° (Co_3O_4) to 36.5° (CoO) and the appearance of the 42.5° line. These lines decrease when the temperature reaches 350°C and disappear at 400°C.

The specific pattern of metallic cobalt appears after reduction at 350°C and its intensity increases with the temperature.

10CoA1 catalyst. Figure 5 shows the diffractograms of the 10CoA1 catalysts *in situ* reduced at 440°C after different pretreatments (airflow calcination, nitrogen-flow calcination, and hydrogen-flow direct reduction of the precursor). The alumina-support contribution to the diffractogram has not been removed, because differences are evident and there is no necessity for substraction of patterns. In this case we observe that even for 440°C

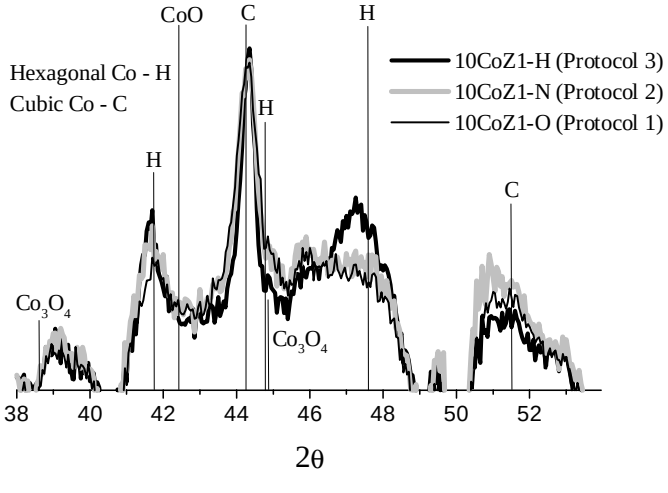

FIG. 3. XRD diagrams of 10CoZ1 catalyst reduced at 450°C in H_2 flow, function of the thermal treatment, after support-pattern subtraction.

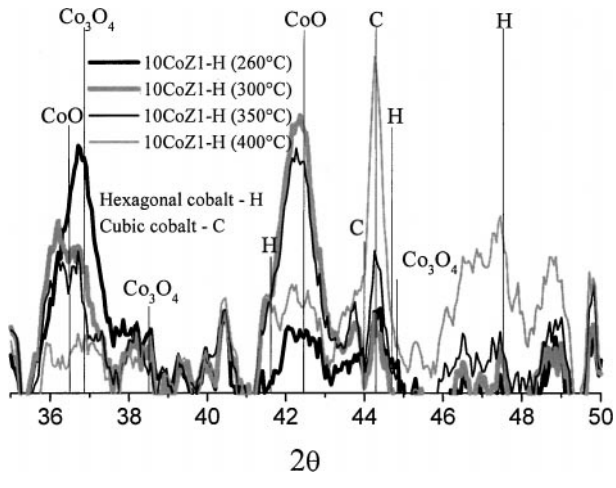

FIG. 4. XRD diagrams of 10CoZ1–H at different reduction temperatures after support-pattern subtraction.

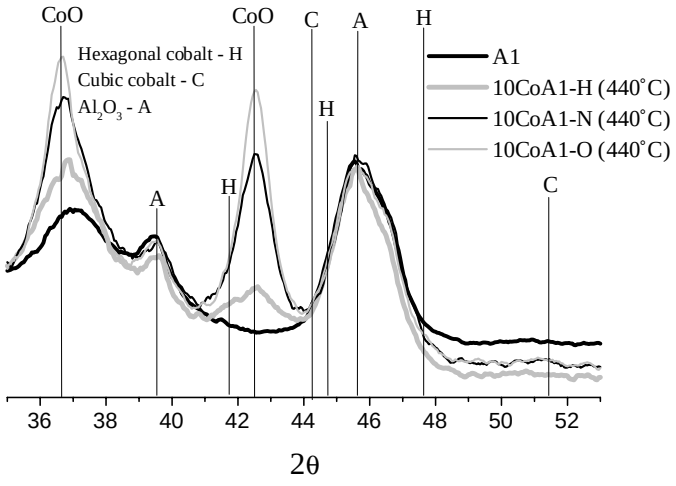

FIG. 5. The effect of the thermal treatment on 10CoA1 catalyst.

reduction temperature, only the CoO pattern is clearly visible. The Co(II) oxide crystalline fraction is a function of the thermal pretreatment the catalyst endured. The same trend as in the case of zirconia-supported catalysts is observed:

- The airflow calcination yields more crystallised CoO than the nitrogen-flow calcination.
- The direct reduction of the nitrate precursor yields more amorphous or microcrystalline CoO.

After reduction at 440°C no metallic cobalt pattern can be observed. The cobalt is therefore microcrystalline or disordered.

3.5. Catalytic Results

The catalytic test was performed under conditions favouring methanation. This kind of test has already been reported in publications, which makes a selection between the different catalysts easier (25, 28). The catalyst activity is therefore stabilised after about 5 h on stream, as we can see in Table 3.

The catalytic results for 10CoZ1 catalyst are reported in Table 4. The conversion levels obtained after airflow calcination (Protocol 1), nitrogen-flow calcination (Protocol 2), and direct nitrate precursor reduction followed by air contact (Protocol 4) are equivalent. The catalyst which has been in contact with air after a direct reduction of the nitrate precursor seems to present a slightly lower CO conversion. This result is consistent with the increase in particle size observed for this sample by XRD, TEM, and oxygen chemisorption. The increase in cobalt particle size is due no doubt to the exothermicity of the cobalt reoxidation observed at the moment of contact with air. The TOF values are equal for the three samples.

Catalysts reduced *in situ* without air contact after the reduction step (Protocols 3 and 5) present much higher CO conversion values. The CO conversion is 50% higher for a heating rate of 5°C/min (Protocol 3) and 100% higher for a heating rate of 1°C/min (Protocol 5). The optimum reduction temperature for obtaining the maximum CO conversion seems to range between 300 and 350°C.

The calcination under nitrogen or air leads to less active catalyst than direct reduction of the cobalt nitrate precursor. Moreover, the influence of the heating rate over the conversion values indicates that the exothermicity generated by the reduction process of the nitrate phase leads to the strengthening of the cobalt-support interactions and has a negative effect on the catalyst performances, as previously described for other type of supports (5, 6, 11).

Concerning the catalytic selectivity in C_{5+}, the differences observed cannot be used to reach a conclusion because of the conditions favouring methanation that we used during the catalytic test.

The catalytic results obtained for the 10CoA1 catalyst are reported in Table 5. The CO conversion is less sensitive to thermal treatment in the case of these alumina-supported catalysts than in the case of zirconia-supported catalysts. However, the same trend is observed: nitrogen-flow calcination leads to a very small increase in the CO conversion,

TABLE 3

Evolution of Function Based on Time on Stream

Activity	50 min	300 min	390 min	480 min
CO conversion	43.0%	32.8%	33.1%	30.5%
C balance	104.0%	100.9%	101.1%	99.0%

TABLE 4

Catalyst 10CoZ1 Performance in Function of the Thermal Treatment

Thermal treatment	c (CO) (%)	S CH_4 (%)	S C_2–C_4 (%)	S C_{5+} (%)	C balance	TOF (s^{-1})
Protocol 1	32.9	35.3	37.7	27.0	100.8	0.033
Protocol 2	34.8	36.8	37.9	25.3	103.5	0.035
Protocol 3	54.6	37.8	38.2	24.0	100.3	0.054
Protocol 4	30.7	35.8	38.2	26.0	102.2	0.037
Protocol 5	71.1	33.2	36.9	29.9	102.9	0.071
Protocol 5a	69.6	39.0	34.9	26.1	103.5	0.069
Protocol 5b	56.9	33.1	37.9	29.1	98.5	0.056

Note. Test conditions: T, 230°C; m_{cat}, 0.4 g; CO/H_2 ratio, 1/9; D_{CO}, 0.63 L/h; D_{H2}, 5.6 L/h, pressure, 0.5 bar. Results obtained after 5 h time on stream. TOF values calculated from XRD particle-size estimation. Protocol 1: Air calcination—400°C (4 h, 10°C/min). Protocol 2: Nitrogen calcination—400°C (4 h, 10°C/min). Protocol 3: Direct hydrogen reduction of the nitrate precursor—350°C (4 h, 5°C/min). Protocol 4: Direct hydrogen reduction of the nitrate precursor—350°C (4 h, 5°C/min), cooled to room temperature under hydrogen flow, then placed in contact with air. Protocol 5: Direct hydrogen reduction of the nitrate precursor—350°C (4 h, 1°C/min). Protocol 5a: 1°C/min to 300°C (4 h). Protocol 5b: 1°C/min to 400°C (4 h).

TABLE 5

Catalyst 10CoZ1 Performance in Function of the Thermal Treatment

Thermal treatment	c (CO) (%)	S CH_4 (%)	S C_2–C_4 (%)	S C_{5+} (%)	C balance	TOF (s^{-1})
Protocol 1	12.4	47.9	33.0	19.1	101.0	0.015
Protocol 2	13.7	47.3	32.2	20.5	100.5	0.016
Protocol 3	16.8	49.3	31.3	19.5	100.2	0.020

Note. Test conditions: T, 230°C; m_{cat}, 0.4 g; CO/H_2 ratio, 1/9; D_{CO}, 0.63 L/h; D_{H2}, 5.6 L/h, pressure, 0.5 bar. Results obtained after 5 h time on stream. TOF values calculated from XRD particle-size estimation.

but the result could be insignificant because it is in the range of the catalytic test statistical errors. The direct reduction of the nitrate precursor also leads to an increase in this parameter.

If we compare the *in situ* XRD and the catalytic results, we observe that the catalytic results are improved when amorphous or poorly organised hexagonal cobalt is promoted. These results indicate that the reaction takes place on the surface defects (corners and edges) of the metallic phase. The more the cobalt is disorganised (hexagonal with stacking faults or amorphous), the more the catalyst activity is enhanced.

At 350°C (the optimum temperature for catalyst activation), all catalyst diffractograms show only CoO and (sometimes, in function of support or thermal treatment) Co_3O_4 patterns. This is the reason we assume that the active phase is formed by metallic cobalt in interaction with CoO (metallic cobalt formed on the outer surface of the CoO crystallites). These results are in agreement with (6).

4. CONCLUSION

Among the preparation protocols we tried, the thermal treatment, which leads to the best catalytic results, is the direct reduction of the nitrate precursor in the reactor. The effect of the pretreatment is higher in the case of zirconia-supported catalyst. The direct reduction of nitrate precursors is even more effective when using a slow-temperature ramping protocol. This phenomenon is explained by the exothermicity of the nitrate reduction. The slower the temperature ramps, the better the heat evacuation, avoiding any increase in cobalt-support interactions or particle agglomeration. The reduction of Co_3O_4 oxide is difficult and leads to an increase of the cubic crystallised cobalt at the expense of amorphous cobalt or hexagonal cobalt with stacking faults. The direct reduction of nitrate precursor increases the quantity of amorphous cobalt or hexagonal cobalt with crystallographic defects, which are active phases in this reaction. At the same time, the direct reduction leads to weaker metal-support interactions than does precalcination of catalysts.

The nitrogen-flow calcination conducts to an intermediate situation. The quantity of crystallised Co_3O_4 is less important than in the case of airflow calcination and it is more reducible.

ACKNOWLEDGMENTS

The authors thank Mrs. K. Esterle for performing the TEM characterisation of the catalysts and Mr. V. Zozaya for his help in the catalytic tests.

REFERENCES

1. Iglesia, E., Soled, S. L., Fiato, R. A., and Via, G. H., *J. Catal.* **143**, 345 (1993).
2. Flory, P. J., *J. Am. Chem. Soc.* **58**, 1877 (1936).
3. Iglesia, E., *Appl. Catal. A* **161**, 59 (1997).
4. Belambe, A. R., Oukaci, R., and Goodwin, Jr., J. G., *J. Catal.* **166**, 8 (1997).
5. Lapidus, A., Krylova, A., Kazanskii, V., Borovkov, V., Rathousky, J., Zukal, A., and Jancalkova, M., *Appl. Catal.* **73**, 65 (1991).
6. Rathousky, J., Zukal, A., Lapidus, A., and Krylova, A., *Appl. Catal.* **79**, 167 (1991).
7. Lapidus, A., Krylova, A., Rathousky, J., Zukal, A., and Jancalkova, M., *Appl. Catal.* **80**, 1 (1992).
8. Yoon, K. E., and Moon, S. H., *Appl. Catal.* **16**, 289 (1985).
9. Ihm, S., Lee, D., and Lee, J., *J. Catal.* **113**, 544 (1988).
10. Fu, L., and Batholomew, C. H., *J. Catal.* **92**, 376 (1985).
11. Iglesia, E., *Appl. Catal. A* **161**, 59 (1997).
12. Reuel, R. C., and Bartholomew, C. H., *J. Catal.* **85**, 78 (1984).
13. Zonneville, M. C., and Geerlings, J. J. C., *J. Catal.* **148**, 417 (1994).
14. Mac Donnald, M. A., Storm, D. A., and Boudart, M., *J. Catal.* **102**, 386 (1986).
15. Iglesia, E., Soled, S. L., and Fiato, R. A., *J. Catal.* **137**, 212 (1992).
16. Geerlings, J. J. C., Zonnevylle, M. C., and de Groot, C. P. M., *Surf. Sci.* **241**, 302 (1991).
17. Ernst, B., Libs, S., Chaumette, P., and Kiennemann, A., *Appl. Catal. A* **186**, 145 (1999).
18. Zhang, Y., Xiang, H., Zhong, B., and Wang, Q., *in* "Proceedings of the 217th National Meeting of the American Chemical Society, Anaheim, CA, March 21–25," p. 88, Am. Chem. Soc., Washington, DC, 1999.
19. Rohr, F., Lindvag, O. A., Holmen, A., and Blekkan, E. A., *Catal. Today* **58**, 241 (2000).
20. Ali, S., Chen, B., and Goodwin, Jr., J. G., *J. Catal.* **157**, 35 (1995).
21. Mouaddib, N., Perrichon, V., and Martin, G. A., *Appl. Catal. A* **118**, 63 (1994).
22. Zhang, Y., Xiang, H., Zhong, B., and Wang, Q., *Pet. Sci. Technol.* **17** (9&10), 981 (1999).
23. Potoczna-Petru, D., and Kepinski, L., *Catal. Lett.* **73**(1), 41 (2001).
24. Fadoni, M., and Lucarelli, L., *in* "Studies in Surface Science and Catalysis." (A. Dabrowski, Ed.), Vol. 120, "Adsorption and Its Applications in Industry and Environmental Protection," pp. 177–225. Elsevier, Amsterdam, 1999.
25. Ducreux, O., Lynch, J., Rebours, B., Roy, M., and Chaumette, P., *Stud. Surf. Sci. Catal.* **119**, 125 (1998).
26. Colley, S. E., Copperthwaite, R. G., Hutchings, G. J., Terblanche, S. P., and Thackeray, M. M., *Nature* **339**, 129 (1989).
27. Sninivasan, R., De Angelis, R. J., Reucroft, P. J., Dhere, A. G., and Bentley, J., *J. Catal.* **116**, 144 (1989).
28. Rohr, F., Holmen, A., Barbo, K. K., Warloe, P., and Blekkan, E. A., *Stud. Surf. Sci. Catal.* **119**, 107 (1998).